Pergamon

Journal of Structural Geology, Vol. 18, No. 11, pp. 1353 to 1367, 1996

PII: S0191-8141(96)00061-2
0191-8141/96 $15.00+0.00

Distribution of angular misfits in fault-slip data

POM-YONG CHOI*

Korea Institute of Geology, Mining and Materials, P.O. Box 111, Yusong Post Office, 30 Kajung-dong, Yusong-gu, Taejon, 305-350, Korea

JACQUES ANGELIER and BLAISE SOUFFACHÉ

Laboratoire de Tectonique Quantitative, Université P. et M. Curie, Boîte 129, T26-25, El, 4 place Jussieu, 75252 Paris Cedex 05, France

(*Received* 6 *March* 1995; *accepted in revised form* 10 *June* 1996)

Abstract—The validity and the accuracy of a stress determination method based on fault-slip data inversion depends on how the misfits are defined and processed in the inversion procedure. To characterize major features of fault-slip data, angular misfits are simulated for both inherited faults and conjugate faults. For one case, a set of 4000 'perfect' fault-slip data was built for the inherited fault type (the general case), with planes randomly distributed on a unit sphere and slip vectors which perfectly fit a given stress tensor. Likewise, a set of 200 'perfect' fault slip data was built for the conjugate fault type, where variations simply occur around two poles. These synthetic fault slip data sets were modified by adding variations of orientations, for both fault planes and slip vectors, according to a Gaussian-type distribution. After re-calculating the stress tensor, we examined the distribution of angular misfits and residuals of five minimization functions (depending on the inversion method adopted), and we evaluated the corresponding variations of the stress tensor.

We found that the distribution type of angular misfits is exponential (or half-Gaussian) for both inherited and neoformed fault populations. Iterative or grid search methods are supposed to correspond to a χ^2 test. The application of a χ^2 test to the stress determinations demands that misfits be described as angular misfits which follow a Gaussian law. Thus, to avoid a theoretical contradiction in these iterative or grid search methods, one must adopt a sum of squares misfit criterion as a minimization function. In that the angular misfits follow an exponential law, the function to minimize the sum of the absolute values of misfits can be also meaningful for the stress inversion.

The four minimization function misfits considered here are also exponential in type, so that our conclusion apparently contradicts the assumption underlying the iterative linear inversion methods derived by least squares method. The use of least squares criteria in fault-slip data inversion implies that the misfits of the minimization function should follow the Gaussian law. Because the three components of residual vectors follow a Gaussian distribution, we suggest that it is theoretically sound to construct elementary minimization functions using them. The usual form of minimization functions is the coalescence of these three elementary minimization functions. The total inversion method is also consistent with it in that its minimization function is the sum of three elementary minimization functions constructed in three angular differences which follow the Gaussian law. The distribution of the minimization function misfits of the direct inversion method is quite different in type, and can be explained by a β-distribution, which reflects the physical characteristics of the criterion adopted.

We evaluated variations in the determined stress tensors as a function of the data dispersion and 'filtering' misfit angle. Under the conditions adopted in this paper, the stress solutions depend on the dispersion parameters, and are stable and vary little for smaller data dispersions. The 'filtering' misfit angle between 45° and 90° is appropriate to reconstruct the assumed stress tensor by including as many meaningful fault-slip data as possible. Copyright © 1996 Published by Elsevier Science Ltd

INTRODUCTION

In the process of stress inversion of fault-slip data for a given tectonic event, the determination of a stress tensor contains a certain amount of error, and the fit between all the data and the single computed stress tensor is an approximation. This common observation is accounted for by (1) the uncertainties of structural measurement values, (2) some geometrical characteristics of fault slips, (3) the basic mechanical assumptions which lead to neglect of stress perturbations in the faulted rock mass, and (4) the adopted specific characteristics of each stress inversion technique.

Since Carey & Brunier (1974) presented first the possibility of stress inversion from fault-slip data, numerous methods for determining stress tensors using fault-slip data or focal mechanisms of earthquakes have been proposed with various approaches (Angelier 1975, 1979, 1984, 1990, 1991, Carey 1976, Etchecopar *et al.* 1981, Angelier *et al.* 1982, Armijo *et al.* 1982, Gephart & Forsyth 1984, Michael 1984, Carey-Gailhardis & Mercier 1987, Reches 1987, Choi 1991, Fleischmann & Nemcok 1991, Yin & Ranalli 1993). An overview of this application of solid mechanics to the stress determination in brittle tectonics was presented elsewhere (Angelier 1994; see also Hancock 1985). All these methods are based on the stress–slip relationship described by Wallace (1951) and Bott (1959); the validity of the basic assumptions was discussed in detail by Dupin *et al.* (1993) and Pollard *et al.* (1993). In detail, the misfit criterion functions of different methods differ widely and so do numerical techniques: the iterative or grid search (Carey & Brunier 1974, Angelier 1975, 1984, Gephart & Forsyth 1984), the direct inversion (Angelier 1990, 1991) and the iterative linear inversion (Choi 1991). Statistical

*Corresponding author: E-mail: cpy@rock25t.kigam.re.kr

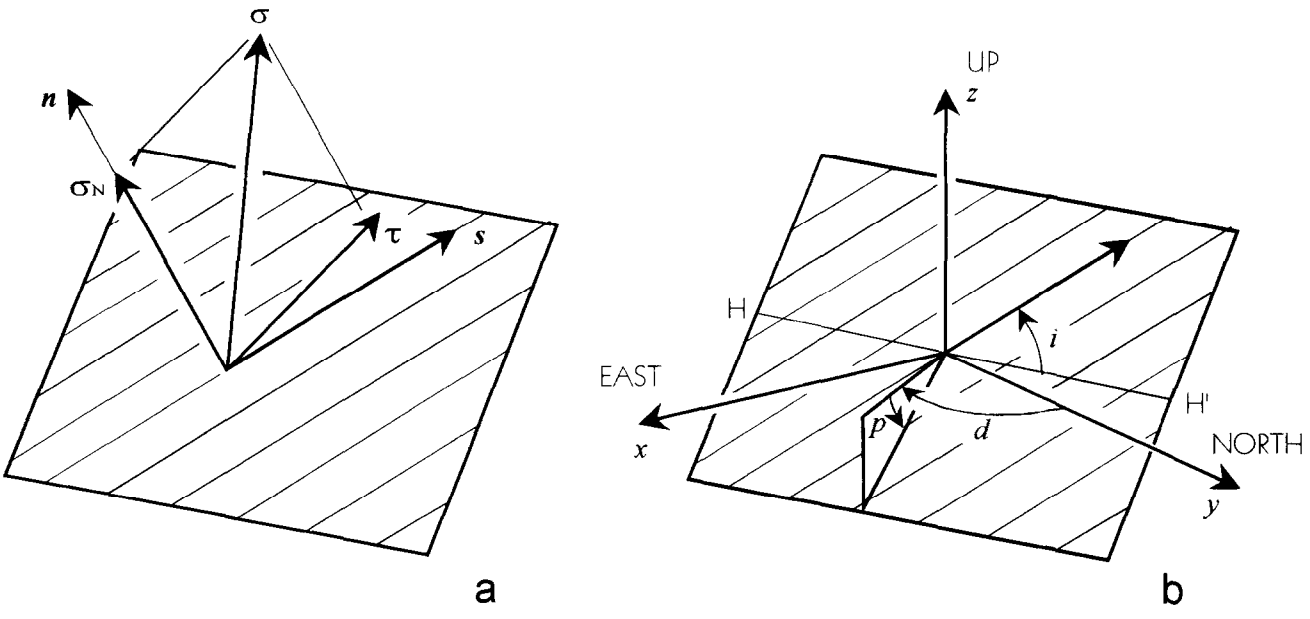

Fig. 1. Diagram showing geometry of a fault-slip and corresponding definitions used in this paper. (a) Geometry of fault plane, slickenside lineations and stresses. **n**: unit vector normal to the fault plane. **s**: unit slip vector on fault plane. σ: stress vector exerted on this fault plane. σ_N: normal component of σ (normal stress). τ: tangential component of σ (shear stress). (b) Geometry of fault and conventional measurements in Ωxyz reference coordinate system. *d*: azimuth of dip direction of fault plane. *p*: dip of fault plane. *i*: pitch of slickensides (modified from Angelier *et al.* 1982).

assumptions also differ, although most authors adopt the least squares criterion (i.e. the sum of the squares of the misfit criterion values is minimized). In all cases, one assumes that the fault-slip direction should coincide with that of shear stress, that the stress state was uniform, and that neither rotation nor volume change occurred during the corresponding tectonic event. The general case is shown in Fig. 1(a), with an angular misfit between the observed slip vector, **s**, and the shear stress, τ, induced by the average stress tensor solution of the problem. This misfit is made as small as possible, but exists due to the errors and uncertainties mentioned above.

The main purpose of this paper is to describe and interpret distribution types of angular misfits and their statistical aspects in the stress inversion, based on extensive computer-assisted modelling. Most fault-slip data sets collected in the field have limited data numbers (e.g. twenty to sixty) and limited ranges of fault orientations. In order to eliminate biases due to inhomogenous distribution, we study statistical characteristics of synthetic fault-slip data sets, which can display all possible orientations, and whose data numbers can be much larger than natural ones. The widely accepted use of the least squares method implies, albeit often in a tacit way, that the residuals of minimization functions are distributed according to the Gaussian law (Linnik 1963). Note, however, that some fault-slip data may have angular misfits far beyond the acceptable level. The distribution may differ from the Gaussian model if such 'anomalous' data are numerous. These data can be rejected if there are reasons to believe that they result from mistakes in observation or classification of measured fault-slip data, or belong to a distinct stress regime (for the separation of stress regimes not discussed herein, see Angelier & Manoussis 1980 and Angelier 1984).

In the stress inversion procedure, we meet a problem: what is the largest misfit angle of fault-slip data acceptable to reconstruct the tectonic stress tensor at a site? Because we assume a fixed reduced stress tensor in our computer modelling, we explore this problem by evaluating variations of stress tensors as a function of data dispersion and 'filtering' misfit angle. We can thus discuss the conditions needed to recover the assumed stress tensor for modified fault-slip data sets. Finally, considering the case of a relatively homogeneous stress regime, it is necessary to address the problem of the real distribution of misfits obtained for a given inversion criterion as a function of usual data uncertainties expected in a fault-slip data set. The distribution of misfits is also examined for five typical minimization functions listed in Table 1, and we will discuss their implications in stress inversion.

ANGULAR DATA AND UNCERTAINTIES

Figure 1(b) illustrates the geometry of the fault slip, which depends on three angles: the dip direction (*d*), the dip (*p*) of the plane, and the pitch (*i*) of the fault striations. Instrumental uncertainty may be as small as 1–2° with high quality equipment, whereas the observational uncertainty commonly averages 5–10°, depending on numerous factors. The three angles *d*, *p* and *i* are considered independent in the first approximation. However, for instance, a small variation in dip (*p*) of a nearly vertical plane may result in an opposite dip direction, hence a large change in dip direction (*d*). Such effects have little influence in statistics, although they must be carefully considered in particular cases.

Figure 2 illustrates some features that significantly

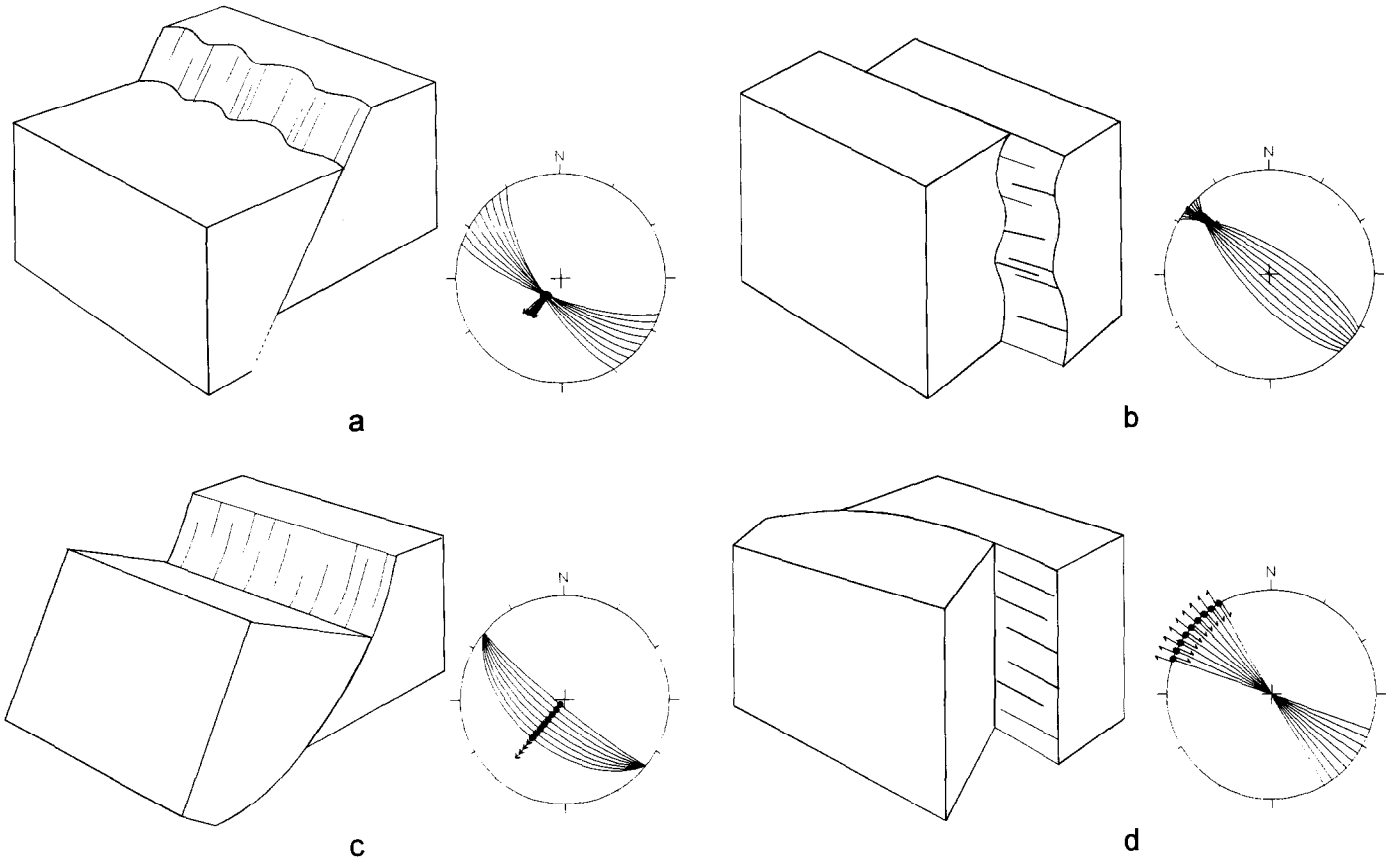

Fig. 2. Examples of particular fault geometries and their influence on strike, dip and pitch angles. (a) Variations around slip vector for a normal fault causing changes in *d*. (b) Variations around slip vector for a strike-slip fault, causing changes in *p*. (c) Variations perpendicular to the slip vector for a normal fault, causing changes in *p*. (d) Variations perpendicular to the slip vector for a strike-slip fault, causing changes in *d*.

contribute to data dispersion, as far as the shape of a fault plane is concerned. The changes around the slip vector (e.g. big grooves) may result in variations in *d* (which imply smaller changes in *p* and *i*) for a dip-slip fault (Fig. 2a), or *p* for a strike-slip fault (Fig. 2b). The changes perpendicular to the slip vector can cause variations in *p* for a dip-slip fault (Fig. 2c), and *d* for a strike-slip fault (Fig. 2d). For the oblique slip faults, the variations are more complicated and there is a wide range of possible variations, all angles *d*, *p* and *i* being affected in varying proportions. As Fig. 1(b) suggests, these three angles vary from 0 to 360° (*d* and *i*), or 0 to 90° (*p*). The corresponding uncertainties range between $-180°$ and $+180°$ (Δd & Δi) or $-90°$ and $+90°$ (Δp).

Now, what is important is which type of distribution law better describes the dispersion of fault-slip data. A Fisher distribution (Fisher 1953, Mardia 1972) is appropriate to describe the clusters of parallel features (e.g. bedding planes, foliations, lineations and possibly dikes) on a unit sphere, and a Watson distribution (Watson 1966) is suitable for the description of the girdle-type distribution of these features. For instance, considering a set of the conjugate faults, one group of this conjugate pair can be described by a Fisher distribution, but both fault groups cannot be treated at the same time by this polar distribution. The fault planes and their slip vectors are not parallel features (Figs. 5a & b), so that the three angles of fault-slip data are dispersed and mutually independent, although they constrain a reduced stress tensor. As for the data dispersion function, it is assumed *a priori* that it must define a distribution with the greatest frequency for smallest angular misfits, which is the case for the Gaussian, the von Mises and the Cauchy distributions (for instance). A von Mises distribution, suitable for circular random variables (Mardia 1972), is also applicable to describe these variations; its general shape is quite similar to that of a Gaussian law. Adoption with numerous actual data sets suggests that where a single tectonic regime is involved, the distribution of misfit angles is compatible with such a distribution, and does not allow distinction between these functions. We consequently adopt a Gaussian (or normal) distribution to describe the data dispersion of these mutually independent angular data (Fig. 3), since it fits examples of data distributions collected in actual sites well and is easy to apply. In addition, we consider that to be consistent with the assumptions underlying the stress inversion methods, it is better to adopt a Gaussian-type law as a data dispersion function. The Gaussian distribution is defined as follows:

$$f(x) = ce^{-(x-\mu)^2/2\sigma^2} \quad \text{with} \quad c = \frac{1}{\sigma\sqrt{2\pi}} \qquad (1)$$

where $f(x)$ is the frequency of the value x, μ is the average ($\mu = 0$ herein), and σ is the standard deviation. For the clarity of description, we apply this function to data

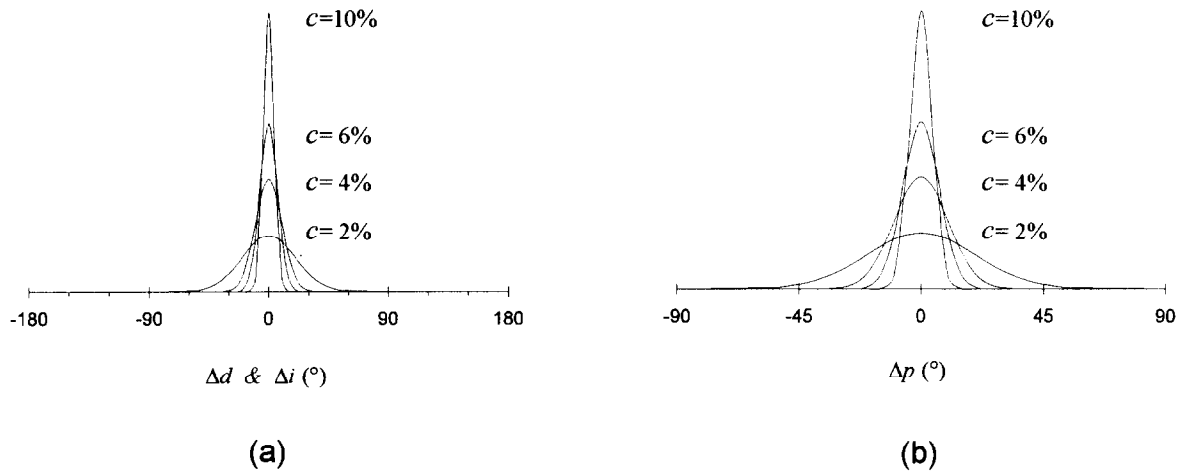

Fig. 3. Gaussian-type distribution of data uncertainties. (a) Data uncertainties of dip direction of fault (Δd) and pitch of slickenside lineations (Δi). (b) Those of dip of fault (Δp). The parameter c is defined in equation (1) of text.

modifications in terms of discrete distribution with a class width of 1°.

As mentioned before, the use of Gaussian distributions requires that the large errors are considered exceptional. This is the case for monophase and homogenous fault-slip data, consistent with a single stress tensor with the range of approximations and uncertainties. The case of polyphase fault sets is always decomposable into analyses of monophase subsets (Angelier & Manoussis 1980). Note also that depending on the minimization criterion adopted, the angular misfit is attributed to the variations in the slip vector (Fig. 4a) or to the three angles considered solely (Fig. 4b), the latter case being represented in the total inversion method (TOTINV, see Table 1).

INVERSION CRITERIA

Because the problem of misfits cannot be examined without regard to the inversion method, it is indispensable to examine some criteria. Table 1 summarizes the minimization functions and their criteria (or estimators) already presented with the corresponding references. Some minimization functions simply refer to the angle between the observed slip vector **s** and calculated shear stress $\boldsymbol{\tau}$(R4DT or R4DS & DAGUR, see Table 1). Other functions include, in addition, the shear stress modulus $|\tau|$, which implies a dimensional parameter whose definition depends on the form of the reduced stress tensor adopted (INVD and BURIAT, see Table 1). The total inversion method minimizes the variations of all angles d, p, i between a 'perfect' theoretical fault slip and measured structural values (TOTINV, see Table 1 and Fig. 4b).

The angular misfit, δ, corresponding to the angle ($\mathbf{s}$, $\boldsymbol{\tau}$), which plays the major role in most minimization functions, has been considered as the main misfit criterion by most authors (e.g. Carey & Brunier 1974, Angelier 1984, Choi 1991). This implies, firstly that the uncertainties affecting fault-plane orientations are considered negligible with respect to the uncertainties affecting the pitch of the slip vector (Fig. 4a, R4DT and R4DS & DAGUR in Table 1), in contrast to the more complex angular misfit criterion of the total inversion (Fig. 4b, TOTINV in Table 1). It also implies that the relative magnitude of the shear stress, $\boldsymbol{\tau}$, is not taken into account, in contrast with the direct inversion (INVD) in

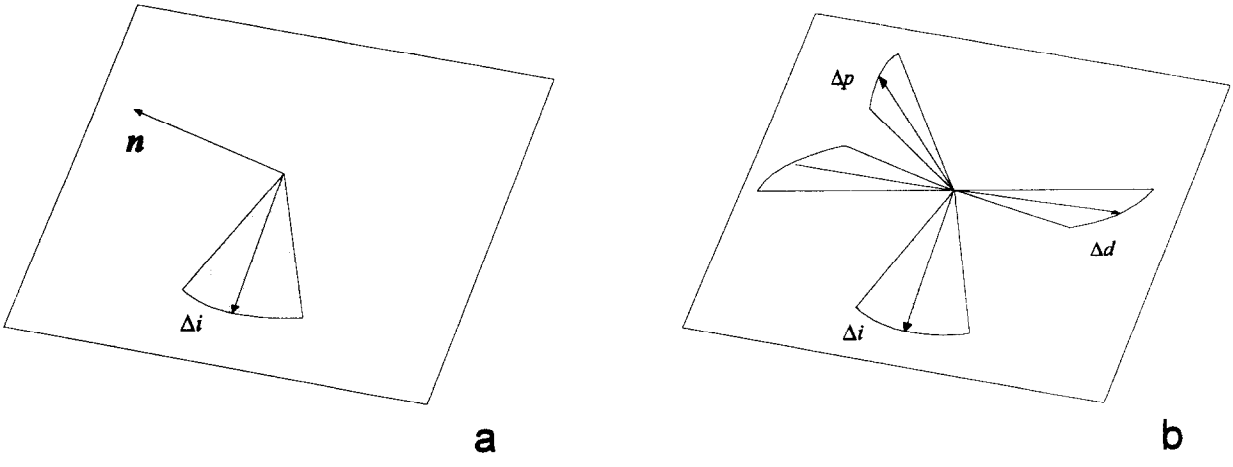

Fig. 4. Range of angular misfits. (a) Plane considered perfect, so that the misfit concerns solely the direction of the slip vector (most methods). (b) Errors on angles d, p and i are all considered (TOTINV, see Angelier *et al.* 1982).

Table 1. Minimization functions and their misfit criteria (or estimators) examined in this paper

Methods	Misfit criteria	Minimization functions
TOTINV Angelier *et al.* (1982)	$C_1 = \left[\left(\frac{d-d^*}{\sigma}\right)^2+\left(\frac{p-p^*}{\sigma}\right)^2+\left(\frac{i-i^*}{\sigma}\right)^2\right]^{1/2}$	$S = \left[\left(\frac{d-d^*}{\sigma}\right)^2+\left(\frac{p-p^*}{\sigma}\right)^2+\left(\frac{i-i^*}{\sigma}\right)^2\right]$
R4DT Angelier (1984)	$C_3 = \min[\tan\delta, 1], (\Delta\mathbf{s} = \mathbf{s}-\boldsymbol{\tau}/\lvert\boldsymbol{\tau}\rvert\cos\delta)$	$S_3 = \Sigma \min[\tan^2\delta, 1]$
R4DS Angelier (1984)	$C_2 = \sin\delta/2$	$S_2 = \Sigma \sin^2\delta/2$
DAGUR Choi (1991)	$\Delta\mathbf{s}_1 = \mathbf{s}-\boldsymbol{\tau}/\lvert\boldsymbol{\tau}\rvert$	$SS_1 = \Sigma[(\tau_x/\lvert\boldsymbol{\tau}\rvert-s_x)^2+(\tau_y/\lvert\boldsymbol{\tau}\rvert-s_y)^2+(\tau_z/\lvert\boldsymbol{\tau}\rvert-s_z)^2] = 4\,\Sigma \sin^2\delta/2$
BURIAT Choi (1991)	$\Delta\mathbf{s}_2 = \lvert\boldsymbol{\tau}\rvert\mathbf{s}-\boldsymbol{\tau}$	$SS_2 = \Sigma[(\tau_x-\lvert\boldsymbol{\tau}\rvert s_x)^2+(\tau_y-\lvert\boldsymbol{\tau}\rvert s_y)^2+(\tau_z-\lvert\boldsymbol{\tau}\rvert s_x)^2] = 4\,\Sigma\lvert\boldsymbol{\tau}\rvert^2 \sin^2\delta/2$
INVD Angelier (1990)	$C_4 = \lvert\lambda\mathbf{s}-\boldsymbol{\tau}\rvert, (\Delta\mathbf{s} = \lambda\mathbf{s}-\boldsymbol{\tau})$	$S_4 = \Sigma(\lvert\lambda\mathbf{s}-\boldsymbol{\tau}\rvert)^2 = \Sigma[\lambda^2+\lvert\boldsymbol{\tau}\rvert^2-2\lambda\lvert\boldsymbol{\tau}\rvert\cos\delta$

Table 1 (see also BURIAT). It is necessary to distinguish the angular misfit, which affects the angle ($\mathbf{s}$, $\boldsymbol{\tau}$), and the misfit criteria, which affect the minimization functions (Table 1). This distinction is especially important for criteria that depend on the relative stress magnitude (see Angelier 1990 for complete discussion). Other differences, which deal with numerical or analytic techniques, have little interest in the analysis of misfits discussed herein.

CONSTRUCTION OF SYNTHETIC DATA SETS

In order to analyze the effects of data dispersion, we first built a perfect data set and then introduced a geometrical dispersion. The synthetic data sets were obtained by generating fault planes in a half-space and computing their slip vectors as a function of an assumed stress tensor. Two situations were considered: the case of pre-existing planes of weakness which may have any orientation (for instance, joints, bedding planes and pre-existing fault planes, etc.) and undergo shear reactivation under the stress regime considered ('inherited faults'; see Fig. 5), and the case of conjugate shear planes, which develop under a given stress regime and thus have particular orientations relative to the stress axes ('neoformed faults' or contemporaneous faults; see Fig. 6).

Note that because the orientation of the stress axes can be chosen arbitrarily, our statistical analysis is carried out in the coordinate frame defined by the stress axes themselves. For the sake of simplicity, we adopt constant stress orientation throughout this paper: σ_1 (maximum compressive stress) in E–W direction (x-axis), and σ_3 (minimum compressive stress) vertical (z-axis). The observed angles for each fault (Fig. 1b) are measured with reference to the horizontal plane. As a result, the effects of dispersion on the three angles d, p and i are not similar depending on the orientations of stress axes and fault patterns. Because a complete presentation of the effects of dispersion for 'normal', 'strike-slip', 'reverse' and 'oblique'-type stress regimes requires a long description, we simply consider in this paper the case with vertical σ_3 solely (Figs. 5 & 6).

Figure 5 illustrates the case of inherited faults with a large variety of orientations: 4000 fault planes were constructed by applying a grid on a Schmidt net and the corresponding strike and dip angles were rounded in degrees. We then computed the shear direction (and sense) for each fault according to the Wallace–Bott hypothesis (i.e. the slip occurs in the direction and sense of the shear stress induced by the single stress tensor adopted). We thus obtained a synthetic set of 'perfect' inherited faults; that is, these 4000 fault-slip data (Fig. 5a & b) have no misfit in terms of the angular deviation between measured slip vector and determined shear stress vector. The determination of the slip vector for each fault is made with the stress axes illustrated in Fig. 5, so that the components of the stress vector, $\boldsymbol{\sigma}$, applied on the plane of unit normal $\mathbf{n}$, are given by:

$$\begin{bmatrix}\sigma_x\\ \sigma_y\\ \sigma_z\end{bmatrix} = \begin{bmatrix}\sigma_1 & 0 & 0\\ 0 & \sigma_2 & 0\\ 0 & 0 & \sigma_3\end{bmatrix}\begin{bmatrix}n_x\\ n_y\\ n_z\end{bmatrix} \quad (2)$$

The components of the shear stress are computed as the differences between the corresponding components of the applied and normal stress vectors:

$$\tau_x = \sigma_x - (n_x\sigma_x + n_y\sigma_y + n_z\sigma_z)n_x$$

$$\tau_y = \sigma_y - (n_x\sigma_x + n_y\sigma_y + n_z\sigma_z)n_y$$

$$\tau_z = \sigma_z - (n_x\sigma_x + n_y\sigma_y + n_z\sigma_z)n_z \quad (3)$$

Finally, the pitch of the computed slip is determined as a function of the shear stress, $\boldsymbol{\tau}$, with reference to the horizontal line in fault plane (Fig. 1). To further simplify the process, we considered a particular relationship between principal stresses, that is, a stress difference ratio $\Phi = (\sigma_2-\sigma_3)/(\sigma_1-\sigma_3)$ (Angelier 1975) of 0.3 (e.g. $\sigma_1 = 1$, $\sigma_2 = 0.3$, $\sigma_3 = 0$). Modifying the value of Φ would result in different slips for most faults.

Figure 6 illustrates the case of neoformed conjugate faults. Note first that a perfect set of conjugate faults includes two fault orientations solely (Fig. 6b), and second that slips on such faults are not influenced by variations in the stress difference ratio Φ. However, because dispersion may occur, variations around theoretical orientations are allowed. In order to reproduce this dispersion, we built 200 fault planes by modifying the fault orientations around the theoretical ones according to the Gaussian law (Fig. 6c), and we determined each shear stress to obtain the 'perfect' slips (Fig. 6d). Because deviations from the two (perfect) orientations of conjugate planes have been imposed, the stress difference

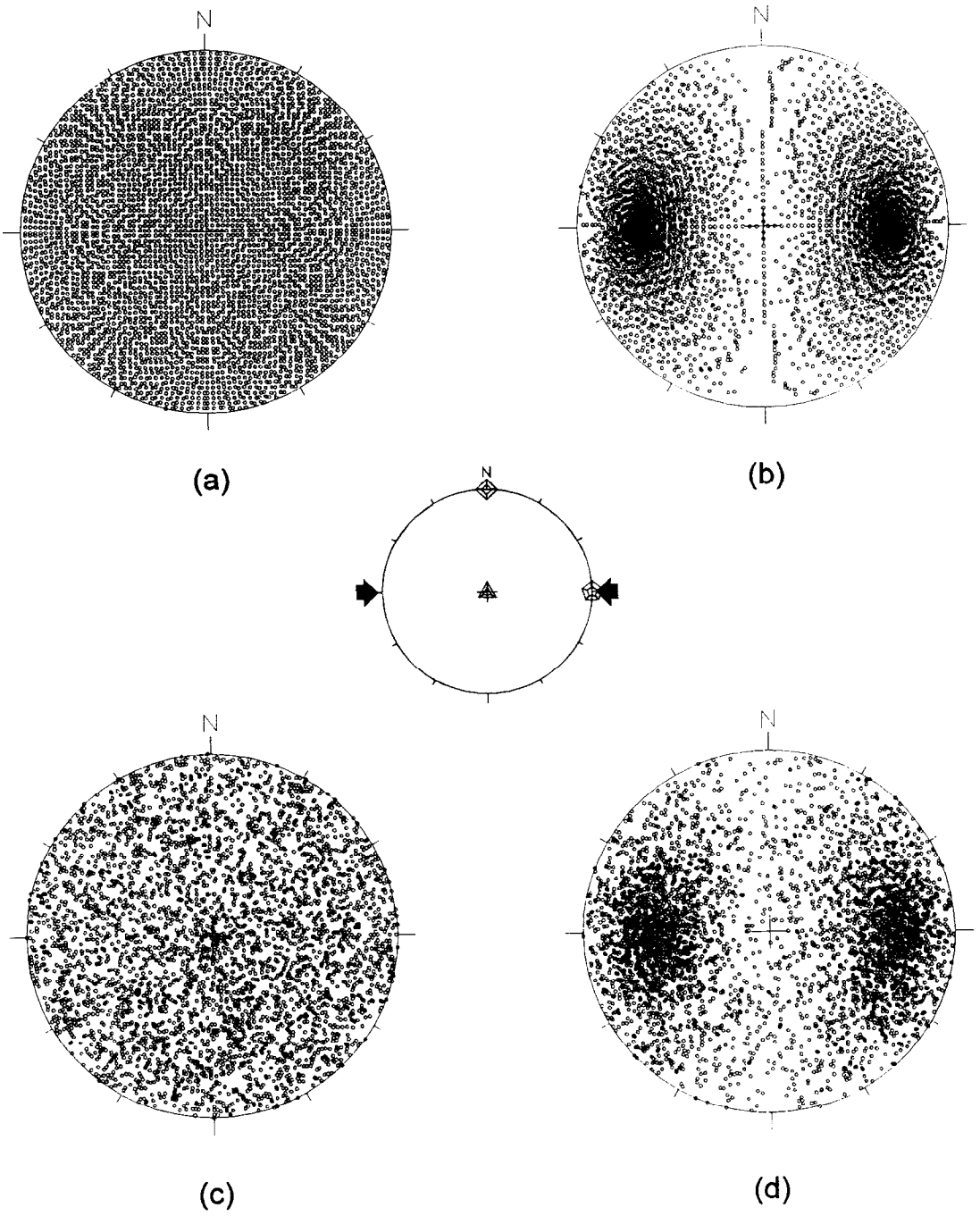

Fig. 5. Poles and striation axes for inherited fault populations. Theoretical set of (a) fault plane poles and (b) slip vector orientations. (c, d) Fault-slip data set from (a) and (b), respectively modified by a geometrical dispersion (c: fault poles, d: slip-vector orientations). $c = 4\%$ is considered.

ratio Φ plays a role in the last step except for the few planes which effectively contain the σ_2 axis, as theoretical conjugate faults should.

INTRODUCTION OF DATA DISPERSION

Dispersion occurs as the result of numerous factors (measurement uncertainties, stress inhomogeneity, irregularities on fault surfaces, fault interaction, deformation due to a later tectonic event, etc.). To simulate this dispersion, following the construction of the 'ideal' sets described above with 4000 (Figs. 5a & b) and 200 (Figs. 6c & d) 'perfect' fault-slip data, we applied individual variations of angles d, p and i to each datum. The amplitude of dispersion is calculated for a class width of 1° by adopting different values for parameter c (equation 1), as illustrated in Fig. 3. The variations introduce individual misfits, but because the populations are large, this dispersion process has relatively little effect on the general agreement between the imposed and the inferred stress tensors (see next section). Finally, we studied the distribution of these misfits, according to several criteria given by various authors (Table 1), in order to determine the relationships between data dispersion and misfit distribution (see later section).

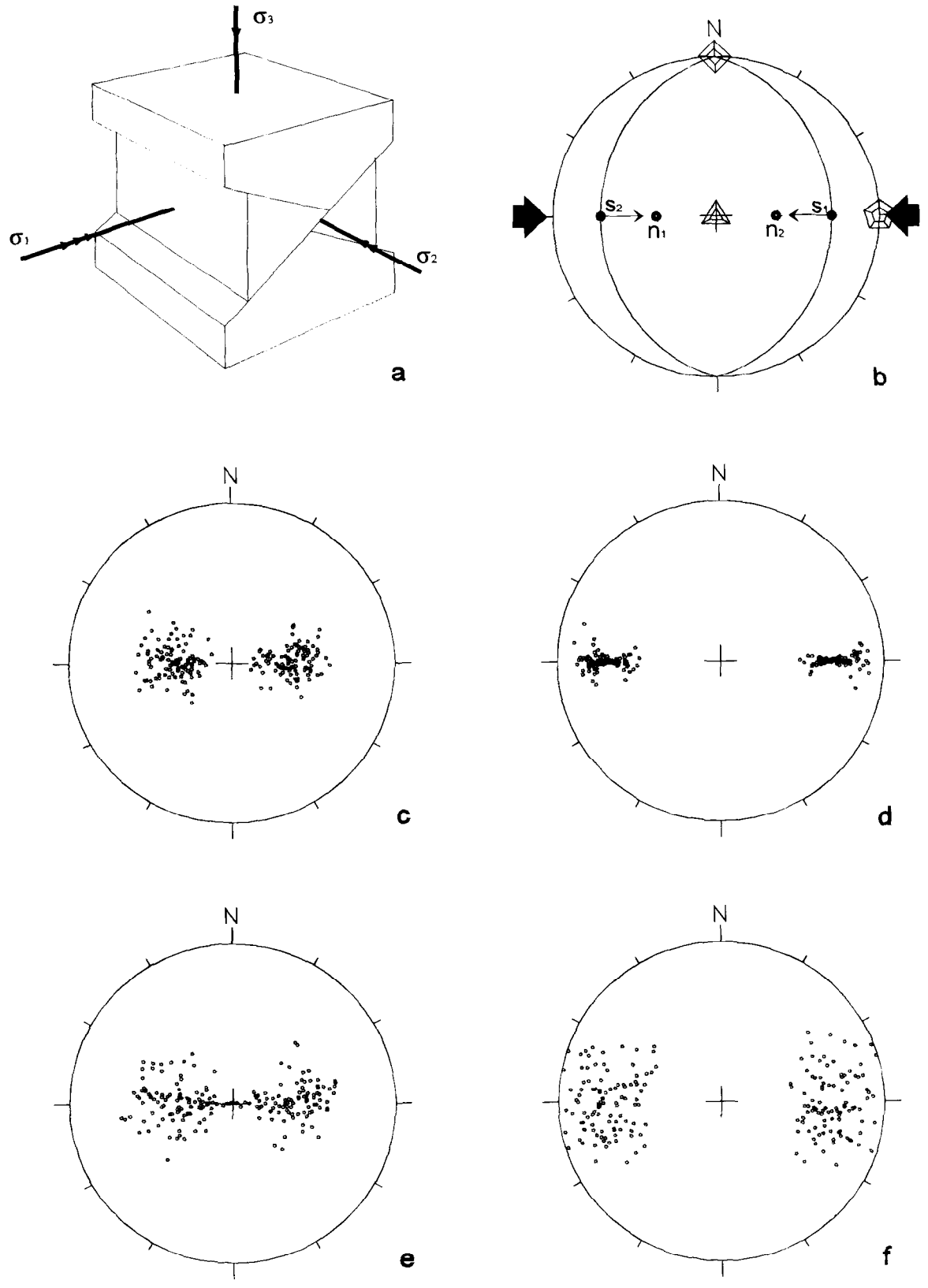

Fig. 6. Schematic diagram showing conjugate faults and modified faults. (a) Block diagram showing a pair of conjugate reverse faults. (b) Fault-plane poles and slip-vector orientations for faults of (a). (c and d) Fault-plane poles (c) and slip vectors (d) of 200 faults constructed by modifying the fault planes and calculating their slip vectors based on the adopted stress tensor. (e and f) Fault-plane poles (e) and slip vectors (f) of modified fault set after dispersion of the theoretical fault set. $c = 4\%$ is considered.

The resulting diagrams of data modifications following a Gaussian law (Fig. 3) are shown in Figs. 5(c) and (d) (poles to faults and slip vectors respectively) for inherited faults and in Figs. 6(e) and (f) (same significance) for conjugate faults. The regular distribution of the initial diagrams is of course altered, as shown by comparisons between Figs. 5(a) and (c) (for fault planes) and between Figs. 5(b) and (d) (for slip vectors) in the case of inherited faults, or between Figs. 6(c) and (e) (for fault planes) and between Figs. 6(d) and (f) (for slip vectors) in case of conjugate faults.

Due to the boundary interactions between d, p, i and their angular changes Δd, Δp, Δi, it is indispensable to consider particular cases (e.g. the reversal of the dip direction d when an initial dip p later becomes larger than 90° after modification and all the modified structural values are transformed in the usual ranges: $0° \leq d < 360°$, $0° \leq p \leq 90°$ and $0° \leq i < 360°$). Note that d^*, p^*, and i^* designate the dip direction, dip, and pitch of the modified faults in Figs. 8–10.

INFLUENCE OF DATA DISPERSION ON DETERMINATION OF STRESS TENSORS

How does the dispersion of fault-slip data affect the resolution of determined stress tensors? We try to determine this influence with respect to the 'filtering' misfit angles (denoted by $\sim$ (s, τ) in Fig. 7) and the parameter c. In stress inversion, fault-slip data with an angular misfit larger than a certain angle are generally considered geologically unacceptable and eliminated; the filtering misfit angle is this maximum misfit angle of fault-slip data in stress inversion. In general, fault-slip data with very large angular misfits (e.g. 90° to 180°) are not used in stress inversion. One generally assumes that they result from mistakes in observation or classification of measured fault-slip data in terms of distinct stress regimes, although their application to the stress inversion is possible in a statistical sense. Angelier (1979), Gephart (1990) and Choi (1991) considered 45° as a realistic filtering misfit angle for including as many meaningful fault-slip data as possible in stress inversion.

To find whether the modified sets are still compatible with the initially adopted stress tensor and to find the appropriate filtering misfit angle acceptable for the recovery of the assumed stress tensor, we tried to determine stress tensors according to the data dispersion parameters, c, and the filtering misfit angles such as 20°, 45°, 60°, 90°, 120° and 180°. For this, we carried out inversion of these modified data sets with the DAGUR and BURIAT methods (Choi 1991). Figure 7 illustrates the variations of principal stress axes, σ_i (denoted by angles $\Delta\sigma_i$ corresponding to the maximum deviation between the assumed and new determined principal stress axes) and those of stress difference ratios, Φ (denoted by values $\Delta\Phi$); the numbers of data applied to the stress inversion are expressed in % with solid lines in figures of $\Delta\Phi$.

Figure 7 shows first that the stress determination depends on data dispersion parameters, c (it is conspicuous for the neoformed fault sets); for low values of c (e.g. $c \leq 3\%$), the change is great as a function of c, while for large values of c (e.g. $c > 6\%$), there is little sensitivity to c values. Second, there is a large contrast between fault types. Angular variations of principal stress axes remain smaller than 5° for inherited fault sets, whereas they reach about 40° for the neoformed fault set of $c = 1.5\%$ (Fig. 7). The variation of the stress difference ratios, Φ, remains stable for $c > 4\%$ with the inherited fault populations, but may be larger for the conjugate fault populations. Both effects are easily explained by considering that fault slips oblique to all stress angles constrain the stress tensor much better (conjugate faults are by definition parallel or approximately parallel to one axis). Third, stress determinations are influenced by the filtering misfit angle. When it is small (e.g. 20°), modified fault-slip data sets may not fit the assumed stress tensor well. If the filtering misfit angle is 45°–90° (and c is greater than 4%), they fit the assumed stress tensor better. For these filtering angles and with $c > 3\%$, approximately 90% of fault-slip data are comprised in the stress inversion. Finally, these differences are also influenced by the adopted stress inversion methods. The stress tensor variations determined by DAGUR are slightly smaller than those by BURIAT especially for $c > 2\%$. In summary, under the conditions adopted in this paper, the solutions depend on the data dispersion, but they are more or less stable for $c > 4\%$. A filtering misfit angle of about 45°–90° is more appropriate to recover the assumed stress tensor than smaller or greater ones.

INTERACTION OF MISFITS WITH DATA UNCERTAINTIES

Let us consider the effects of data dispersion, which of course require reference to a given criterion (Table 1) in order to determine the misfits. The angular misfit δ is determined with respect to the best-fit stress tensor (which in our case is the same as the adopted stress tensor as mentioned above). Considering each criterion for misfit between measured slip vector and determined shear stress vector (as listed in Table 1), we determined the theoretical shear direction on each plane, hence the individual misfit. Again, a stress tensor being given, it is important to distinguish the misfit estimator, which depends on the criterion adopted, and the misfit angle δ, which does not (except for the total inversion). The frequency distribution of misfit angles are described in histograms of Figs. 8 & 9, with a class width of 1°.

Figure 8 (for the inherited faults of Figs. 5c & d) and Fig. 9 (for the neoformed faults of Figs. 6e & f) illustrate the distributions of angular misfits for typical values of c. Better statistical determinations are obtained for the inherited faults, due to the larger number of data (4000 instead of 200). Analysis of these histograms reveals that the frequency distribution of angular misfit can be satisfactorily accounted for by an exponential relationship: $f(\delta) = ae^{-b\delta}$.

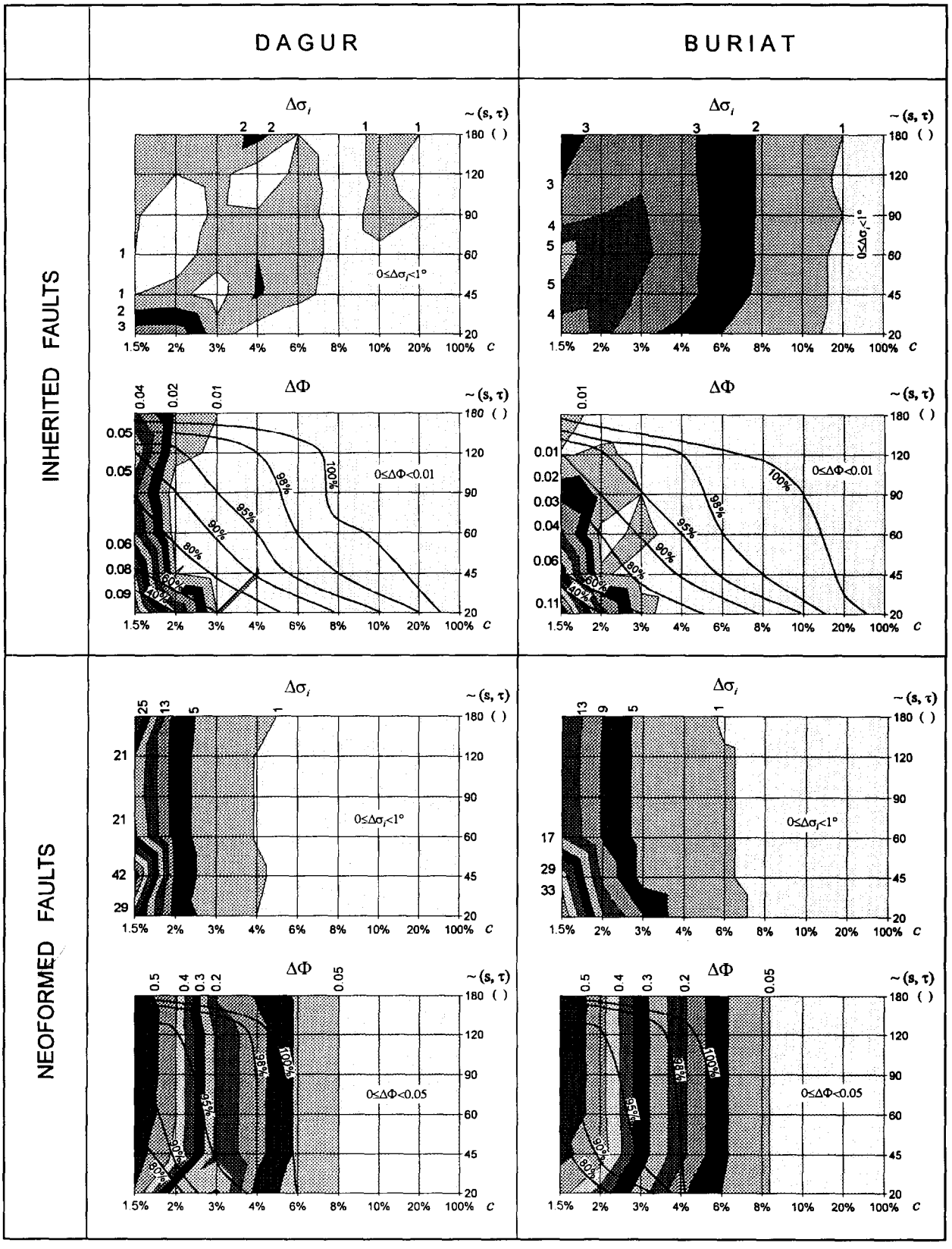

Fig. 7. Variations of stress tensors according to data dispersions and filtering misfit angles. The variations of principal stress axes are found in terms of filtering misfit angles, ~ (s, τ) and parameters, c, according to two stress inversion methods DAGUR (the same minimization function as R4DS) and BURIAT (Choi 1991).

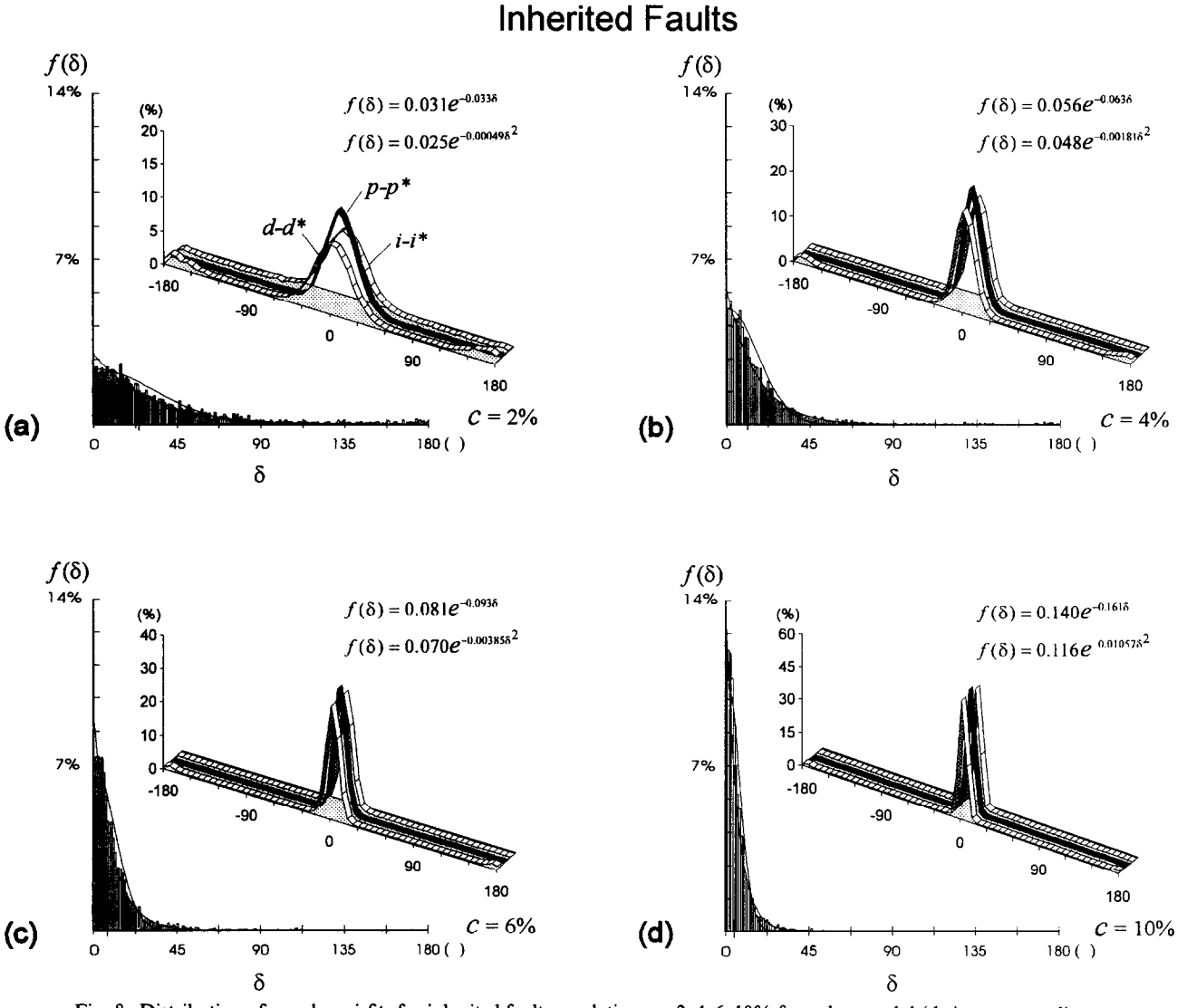

Fig. 8. Distribution of angular misfits for inherited fault populations. c: 2–4–6–10% for a, b, c, and d (their corresponding standard deviations are 20°, 10°, 6.6°, 4°, respectively). Dispersion of angles d, p and i also illustrated. Histogram (b) corresponds to Figs. 5(c & d). δ: median value of each class of angular misfits. $f(\delta)$: frequency of each interval.

Changes in class width do not modify this conclusion. With a class width of 1° (Fig. 8), numerical adjustments resulted in the following values: $b = 1.638c$, and $a = 1.430c = 0.874b$; one thus obtains:

$$f(\delta) = 0.874\frac{e^{-(\delta/\beta)}}{\beta} \quad \text{with} \quad \beta = \frac{0.6105}{c} \tag{4}$$

Figure 8 also shows the numerical fit of the same data with a symmetric distribution function corresponding to the relationship $f(\sigma) = ae^{-b\sigma^2}$ ($\delta \geq 0$):

$$f(\delta) = \frac{2}{\sigma\sqrt{2\pi}}e^{-\delta^2/2\sigma^2} \tag{5}$$

The fit with a half-Gaussian distribution is almost equally satisfactory as that with an exponential distribution.

We also examined distributions of the values for minimization function misfits with various functions in Table 1 (Fig. 10). This determination is shown for the criteria of six different methods, and the frequency distribution modes are analyzed in Fig. 11. Summarizing, for the three minimization functions (R4DT, R4DS & DAGUR, and BURIAT), a good fit is obtained with a negative exponential distribution (the same as for the angular misfits). For the total inversion (TOTINV), the histogram is so narrow that the distribution type remains undetermined (Fig. 10e), but we assume it is similar to that of the upper minimization functions. Note that three components, Δx, Δy, Δz, of the residual vectors (denoted by $\Delta\mathbf{s}$, $\Delta\mathbf{s}_1$ or $\Delta\mathbf{s}_2$ in Table 1) for these four minimization functions follow a Gaussian law. The misfit distribution of the direct inversion method (INVD) is different in type, and could be satisfactorily fitted to a β-distribution (better than Gaussian or Maxwell distributions, see Fig. 11d). Note that this difference in frequency distribution mode corresponds to a difference in nature of the function, which takes the relative shear stress magnitude into particular account for the direct inversion method (Angelier 1990).

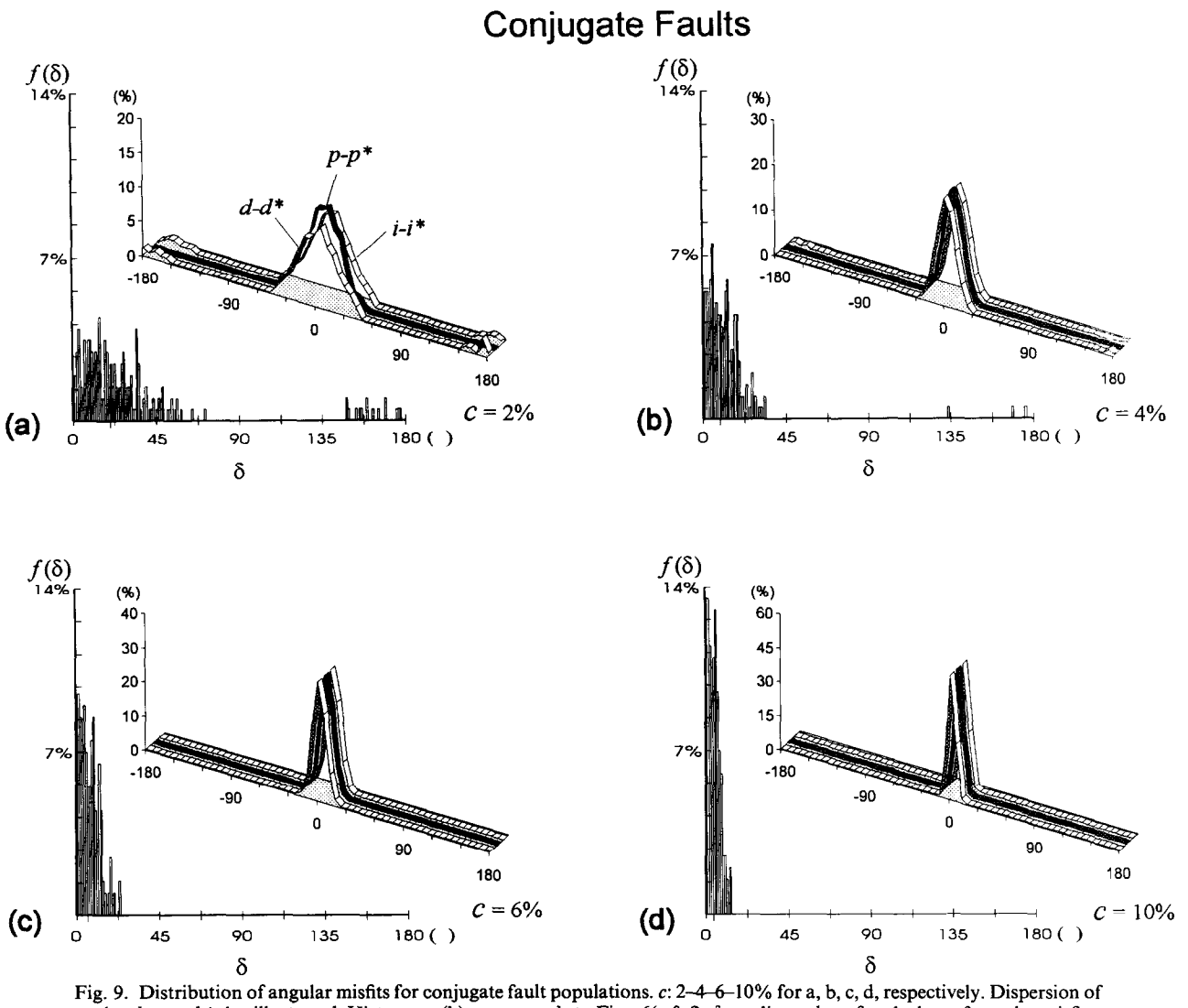

Fig. 9. Distribution of angular misfits for conjugate fault populations. c: 2–4–6–10% for a, b, c, d, respectively. Dispersion of angles d, p, and i also illustrated. Histogram (b) corresponds to Figs. 6(e & f). δ: median value of each class of angular misfits. $f(\delta)$: frequency of each interval.

DISCUSSION AND CONCLUSION

In the stress inversion of fault-slip data, an important problem consists of dealing with the angular misfits, determining a best-fit stress tensor with a data set perturbed by many factors, and determining how far data uncertainties affect the resolution of the stress tensor determinations. We tried to find some answers by simulating the angular misfits as a function of data dispersion, based on analyses of synthetic fault-data sets which allow considerations of all possible orientations (which is not the case for real data sets).

According to the determinations of angular misfit distribution modes (Figs. 8 & 9), we conclude that an exponential frequency function (or maybe a half-Gaussian one) accounts well for the angular misfits with inherited fault populations. For conjugate fault populations, the distribution of angular misfits is thought to be exponential, as is the case for inherited faults, according to a numerical fit between observed and theoretical distributions. These conclusions are not only obtained for the synthetic data sets discussed in this paper but also for real data sets, as the example in Fig. 12 shows. We consider angular misfit in terms of shear stress–slip vector relationship on a fault (Fig. 4a). However, it must be pointed out that we can also calculate the angular difference $i-i^*$ (e.g. Yin & Ranalli 1993), including negative values, which enables a Gaussian distribution to be drawn (Fig. 12b). In any case, the resulting distribution mode of angular misfits is the same as the distribution mode usually observed from real data sets (e.g. Armijo *et al.* 1982, Carey-Gailhardis & Mercier 1987, Gephart 1990 and see Fig. 12a).

Concerning the iterative or grid search methods which aim at minimizing a simple function of the stress–slip angle (Carey & Brunier 1974, Angelier 1975, 1984, Gephart & Forsyth 1984), the determination procedure of the best-fit stress solution is supposed, albeit often in a implicit way, to correspond to a χ^2 test with one degree of freedom. Effectively, one determines in most cases a stress tensor for which the sum of the squares of misfits described by angular misfits is minimum. The applica-

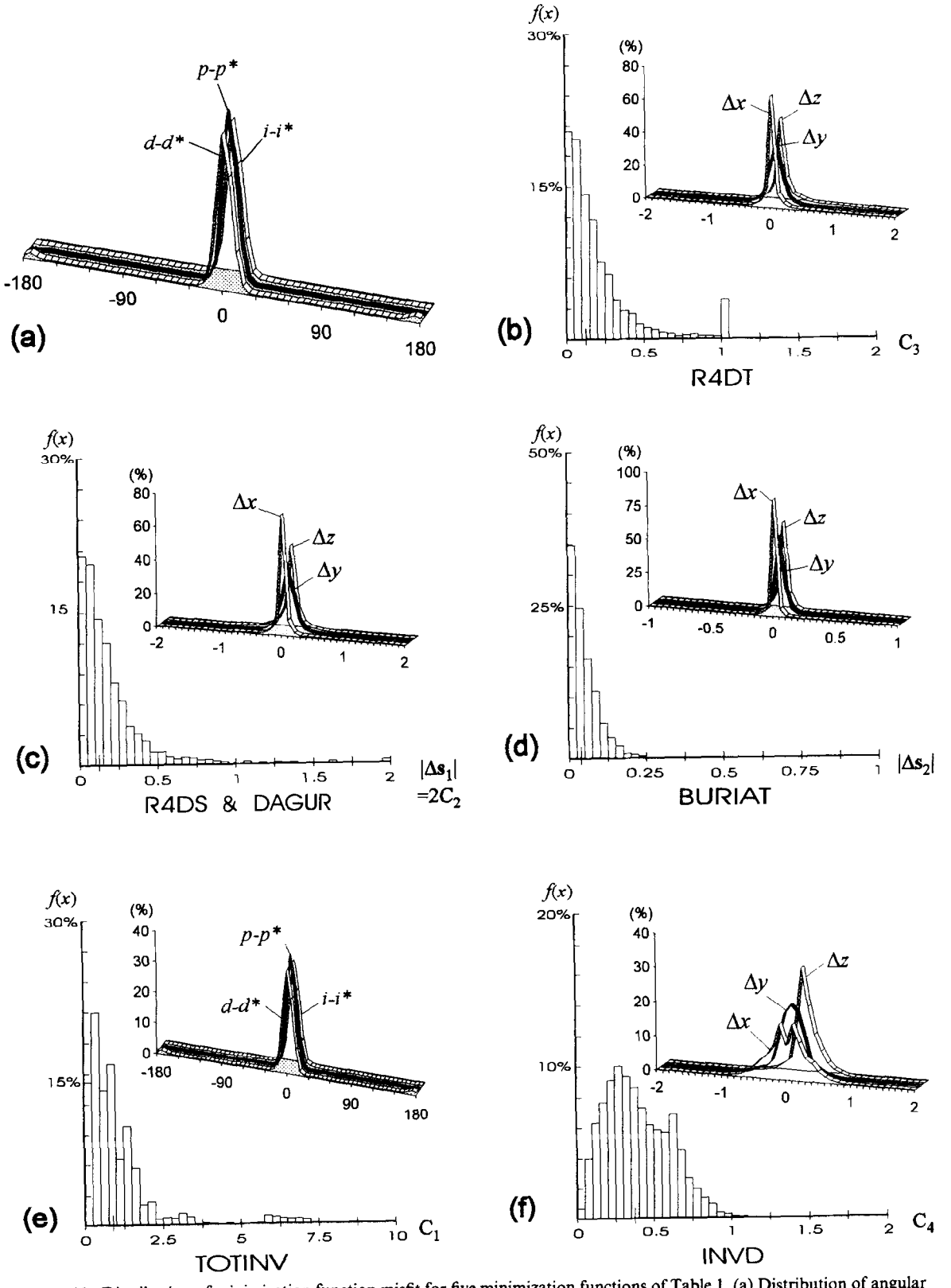

Fig. 10. Distribution of minimization function misfit for five minimization functions of Table 1. (a) Distribution of angular misfits $d-d^*$, $p-p^*$ and $i-i^*$. (b–f) Misfit distributions of each minimization function (see Table 1 for explanation of the criteria). For each histogram, the inset diagrams indicate the distribution of the three components, Δx, Δy, Δz, of the misfit vectors (denoted by Δs, Δs_1 or Δs_2 in Table 1; same data as Fig. 8c).

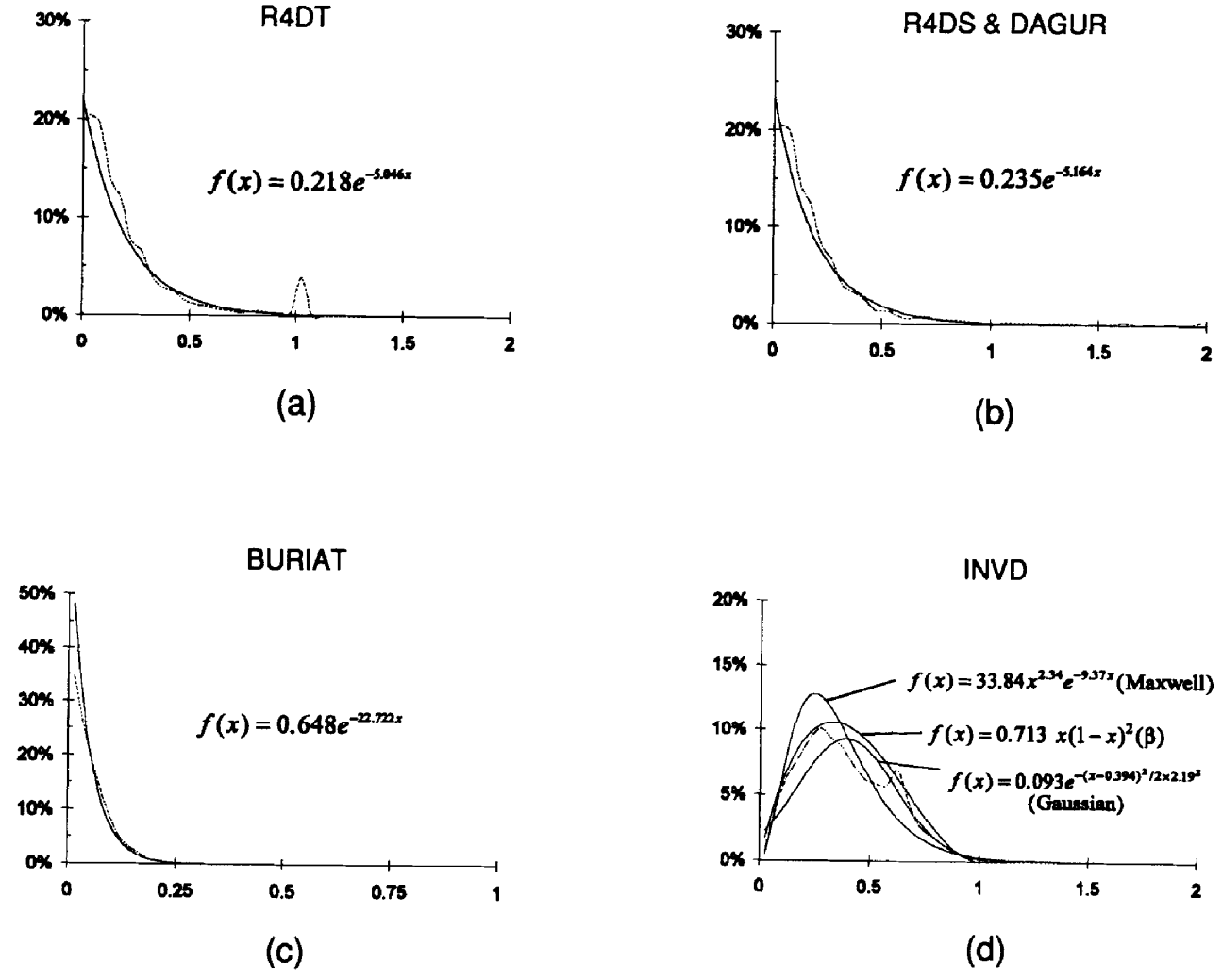

Fig. 11. Distribution type of five minimization functions. (a–c) The three criteria show negative exponential distribution. (d) The distribution of INVD is fitted to three types: Gaussian, β- and Maxwell distributions. The best fit is obtained with the β-distribution. Dashed lines: obtained data. Solid lines: fitted distributions.

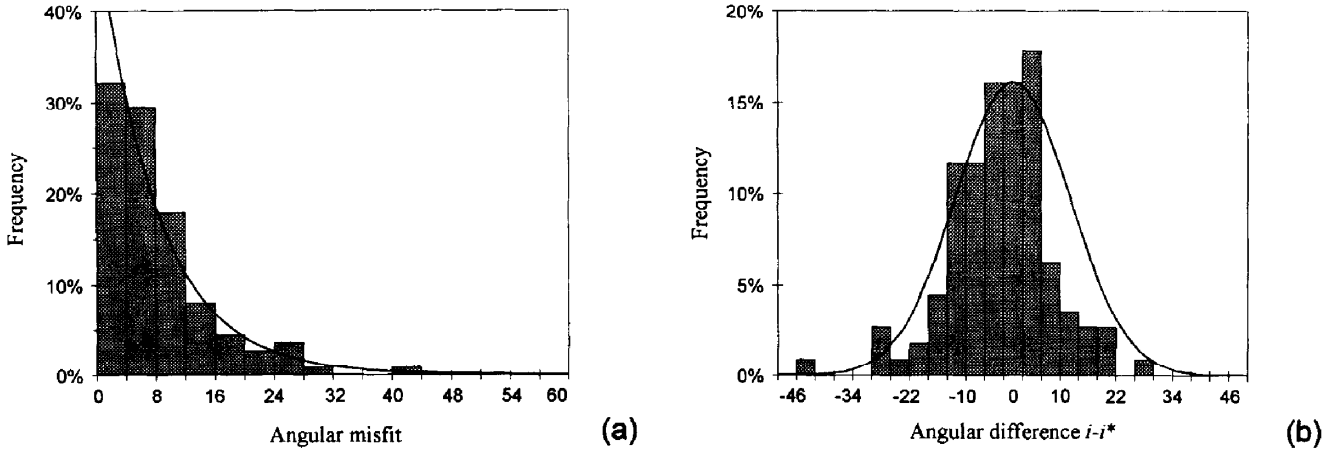

Fig. 12. Distribution of angular misfits (a) and angular differences (b) for a real fault-slip data set. The fault-slip data (the data number is 112) were measured at the site of Yusu-ri, Chinyang-gun, southeastern Korea.

tion of a χ^2 test to the stress determinations demands that misfits described in terms of angular misfits follow a Gaussian law. In order that theoretical contradiction does not occur in these iterative or grid search methods, the sum of the squares of the angular misfits should be adopted as a minimization function. Note, however, that the minimization function might also ignore this aspect. In that the angular misfits do not follow a Gaussian law but an exponential law (or a half-Gaussian one), the function to minimize the absolute value of the sums of misfits described by angular misfits can also be meaningful for the stress inversion (Gephart 1990).

The reconstructed distribution of four minimization function misfits considered here (R4DT, R4DS & DAGUR, BURIAT and TOTINV, see Table 1) is also consistent with an exponential law. As for iterative linear inversion methods, one determines a stress tensor based on the stress equations derived from the minimization functions by the least squares method. For the least squares method, one supposes that the misfits of the minimization function follow the Gaussian law, while our conclusion may seem contrary to it. Knowing that the three components, Δx, Δy, Δz, of the residual vectors of misfit criteria follow a Gaussian distribution (Fig. 10), the minimization functions constructed in terms of each component of residual vectors seem more theoretically sound (e.g. $SS_{1x} = \Sigma(\tau_x/|\tau| - s_x)^2$, $SS_{1y} = \Sigma(\tau_y/|\tau| - s_y)^2$, $SS_{1z} = \Sigma(\tau_z/|\tau| - s_z)^2$ as seen in the minimization function form of DAGUR, see Table 1); this type of minimization function is named an elementary minimization function. Now, we can see that the usual form of minimization functions is the coalescence of these three elementary minimization functions (e.g. DAGUR and BURIAT, Choi 1991). The total inversion (TOTINV) follows this characteristic in that its minimization function is the sum of the three elementary minimization functions constructed in three angular differences $d-d^*$, $p-p^*$, $i-i^*$ which follow the Gaussian law (Figs. 8–10).

The distribution of misfits of the direct inversion method (INVD) is quite different in type (Figs. 10f and 11d), and may be explained by a β-distribution. In fact, the simple minimization by the angle $(\mathbf{s}, \boldsymbol{\tau})$ results in the largest number of smaller misfits, for small angles are abundant provided that the fault-slip data set is homogeneous. The minimization of both angle and difference between the maximum possible shear stress and the computed shear stress results in the particular shape shown in Figs. 10(f) and 11(d), for the shear stress corresponding to the best possible fit generally differs markedly from the largest possible shear stress, $\frac{1}{2}(\sigma_1 - \sigma_3)$. The β-distribution obtained for the direct inversion method thus reflects the physical characteristics of the criterion adopted. Incidentally, this particular case shows that while computing the distribution of misfit residuals based on the reasonable assumption of a Gaussian distribution of angular data uncertainties, one does not just obtain what is put in; the distribution of this method is clearly non-Gaussian contrary to the data uncertainty distribution.

We determined the variations of stress tensors according to data dispersion and found the appropriate filtering misfit angles which allow us to recover the assumed stress tensor. Under the conditions adopted in this paper, the stress solutions depend on the dispersion parameters, but are stable and vary little for $c > 4\%$. Considering the minimization conditions of the angular minimization functions, it is of course preferable to adopt fault-slip data of smaller angular misfits. However, our conclusion is that the filtering misfit angles between 45° and 90° are better to recover the assumed stress tensor concurrently, comprising as many meaningful fault-slip data as possible (more than almost 90% of all fault-slip data for $c > 3\%$), although the stress solutions are governed principally by the data dispersions (Fig. 7).

Acknowledgements—We thank R. J. Twiss, D. A. Ferrill and J. W. Gephart from whose reviews of the manuscript have greatly benefitted it. This work is made within the frame of cooperation in Earth Sciences between France and Korea, sponsored by the French Embassy, the KIGAM and the CROUS, and benefits from the help of the IFP.

REFERENCES

Angelier, J. 1975. Sur l'analyse de mesures recueillies dans des sites faillés: l'utilité d'une confrontation entre les méthodes dynamique et cinématique. *C. R. Acad. Sci. Paris* **281**, 1805–1808.

Angelier, J. 1979. Determination of the mean principal directions of stresses for a given fault population. *Tectonophysics* **56**, T17–T26.

Angelier, J. 1984. Tectonic analysis of fault-slip data sets. *J. geophys. Res.* **89**, 5835–5848.

Angelier, J. 1990. Inversion of field data in fault tectonics to obtain the regional stress—III. A new rapid direct inversion method by analytical means. *Geophys. J. Int.* **103**, 363–376.

Angelier, J. 1991. Inversion directe et recherche 4-D: comparaison physique et mathématique de deux modes de détermination des tenseurs des paléocontraintes en tectonique de failles. *C. R. Acad. Sci. Paris* **312**, 1213–1218.

Angelier, J. 1994. Paleostress analysis of small-scale brittle structures. In: *Continental Deformation* (edited by P. L. Hancock), Pergamon Press, Oxford, 53–100.

Angelier, J. & Manoussis, S. 1980. Classification automatique et distinction des phases superposées en tectonique de failles. *C. R. Acad. Sci. Paris* **290**, 651–654.

Angelier, J., Tarantola, A., Valette, B. & Manoussis, S. 1982. Inversion of field data in fault tectonics to obtain the regional stress—I. Single phase fault populations: a new method of computing the stress tensor. *Geophys. J. R. astr. Soc.* **69**, 607–621.

Armijo, R., Carey, E. & Cisternas, A. 1982. The inverse problem in microtectonics and the separation of tectonic phases. *Tectonophysics* **82**, 145–160.

Bott, M. H. P. 1959. The mechanics of oblique slip faulting. *Geol. Mag.* **96**, 109–117.

Carey, E. 1976. Analyse numérique d'un modèle mécanique élémentaire appliqué à l'étude d'une population de failles: Calcul d'un tenseur moyen des contraintes à partir des stries de glissement (*Unpublished Thesis* of third degree), Tectonique Générale, Université Paris-Sud.

Carey, E. & Brunier, B. 1974. Analyse théorique et numérique d'une modèle mécanique élémentaire appliqué à l'étude d'une population de failles. *C. R. Acad. Sci. Paris* **279**, 891–894.

Carey-Gailhardis, E. & Mercier, J. L. 1987. A numerical method for determining the state of stress using focal mechanisms of earthquake populations: application to Tibetan teleseisms and microseismicity of Southern Peru. *Earth Planet. Sci. Lett.* **82**, 165–179.

Choi, P.-Y. 1991. Method for determining the stress tensor using fault slip data. *J. geol. Soc. Korea* **27**, 383–393.

Dupin, J.-M., Sassi, W. & Angelier, J. 1993. Homogenous stress hypotheses and actual fault slip: a distinct element analysis. *J. Struct. Geol.* **15**, 1033–1043.

Etchecopar, A., Vasseur, G. & Daignieres, M. 1981. An inverse

problem in microtectonics for the determination of stress tensors from fault striation analysis. *J. Struct. Geol.* **3**, 51–65.

Fisher, R. A. 1953. Dispersion on a sphere. *Proc. R. Soc.* **A217**, 295–304.

Fleischmann, K. H. & Nemcok, M. 1991. Paleostress inversion of fault-slip data using the shear stress solution of Means (1989). *Tectonophysics* **196**, 195–202.

Gephart, J. W. 1990. Stress and the direction of slip on fault planes. *Tectonics* **9**, 845–858.

Gephart, J. W. & Forsyth, D. W. 1984. An improved method for determining the regional stress tensor using earthquake focal mechanism data: Application to the San Fernando earthquake sequence. *J. geophys. Res.* **89**, 9305–9320.

Hancock, P. L. 1985. Brittle microtectonics: principles and practice. *J. Struct. Geol.* **7**, 437–457.

Linnik, Y. V. 1963. *Méthode des moindres carrés: éléments de la théorie du traitement statistique des observations* (translated into French by O. Arkhipoff). Dunod, Paris.

Mardia, K. V. 1972. Statistics of directional data, Academic Press, London/New York, 375 pp.

Michael, A. 1984. Determination of stress from slip data: faults and folds. *J. geophys. Res.* **89**, 11517–11526.

Pollard, D. D., Salitzer, S. D. & Rubin, A. M. 1993. Stress inversion methods: are they based on faulty assumptions? *J. Struct. Geol.* **15**, 1045–1054.

Reches, Z. 1987. Determination of the tectonic stress tensor from slip along faults that obey the Coulomb yield condition. *Tectonics* **6**, 849–861.

Wallace, R. E. 1951. Geometry of shearing stress and relation to faulting. *J. Geol.* **59**, 118–130.

Watson, G. S. 1966. The statistics of orientation data. *J. Geol.* **74**, 786–797.

Yin, Z.-M. & Ranalli, G. 1993. Determination of tectonic stress field from fault slip data: toward a probabilistic model. *J. geophys. Res.* **98**, 12165–12176.